J Mol Model (2009) 15:567–572
DOI 10.1007/s00894-008-0425-6

ORIGINAL PAPER

First principles calculations on the influence of water-filled cavities on the electronic structure of Prussian Blue

Jacek C. Wojdeł

Received: 25 August 2008 / Accepted: 11 November 2008 / Published online: 12 December 2008

Abstract Prussian Blue is a paradigmatic mixed valence material and a parent compound to a broad family of electronically, optically, and magnetically active materials. Its exact composition varies greatly depending on the preparation route, leading to large variations in its electronic properties. The influence of water molecules on the structural and electronic properties of Prussian Blue were studied using state-of-the-art first principles calculations. Water-filled cavities were found to have a profound influence on the band gap and density of states of this material while simultaneously leaving many of its properties largely unchanged. The resulting model of an almost independent superimposition of dehydrated material and hydrated sites is briefly discussed.

Keywords Band structure · DFT+U · Hydration · Prussian Blue

Introduction

Prussian Blue (PB) is a crystalline ionic salt formed from the reaction of $[Fe(H_2O)_6]^{3+}$ and $[Fe(CN)_6]^{4-}$ ions in an aqueous environment [1]. It is a mixed valence material in which Fe^{2+} and Fe^{3+} cations coexist at separate face-centred-cubic (fcc) crystalline frameworks, connected by cyanide ligands [1, 2]. Its characteristic deep blue colour arises from the *d*-electron charge transfer between neighbouring Fe sites of different oxidation states. This charge transfer is an excitation with a corresponding broad absorption peak around 1.75 eV [2, 3]. In addition to differences in oxidation, the Fe centres also exhibit different spin states, where carbon-coordinated Fe^{2+} and nitrogen-coordinated Fe^{3+} are in local low-spin and local high-spin configurations, respectively [1, 2, 4]. Charge neutrality of the material is assured by either inclusion of an interstitial cation (usually an alkali metal), or by formation of water-filled cavities. These two different ways of balancing the charge in the unit cell lead to two distinct stoichiometries: $M^{I}Fe[Fe(CN)_6]$ and $Fe_4[Fe(CN)_6]_3{\cdot}nH_2O$ (see Fig. 1), which are commonly referred to as "soluble" and "insoluble" forms of PB respectively—though not directly related to their solubility in water.

PB is a remarkable material because of its complicated nature—in which the structural, electronic, magnetic and optical properties are very closely related—but also because of the fact that it is a parent material to a broad family of PB analogues [1, 5, 6]. The properties of PB can be tailored by electrochemical interchange of interstitial cations, or by substitution of Fe by other transition metals [7]. This freedom in choice of material composition has lead to the synthesis of a variety of materials with potential electro-optical device applications [7, 8]. Furthermore, the magnetic properties of PB analogues are also affected by the same changes, and lead to materials with interesting magnetic properties [9–13]. Additionally, PB is an intrinsic semiconductor, but its finite temperature bulk conductivity can be changed by orders of magnitude by changing the amount of hydration of the sample, or by electrochemical

J. C. Wojdeł
Department de Química Física and Institut de Química Teórica i Computational, (IQTCUB), Universitat de Barcelona,
C/Martí i Franquès 1,
08028 Barcelona, Spain

Present address:
J. C. Wojdeł (✉)
Institut de Ciència de Materials de Barcelona (ICMAB-CSIC),
Campus UAB,
08193 Bellaterra, Spain
e-mail: jcwojdel@icmab.es

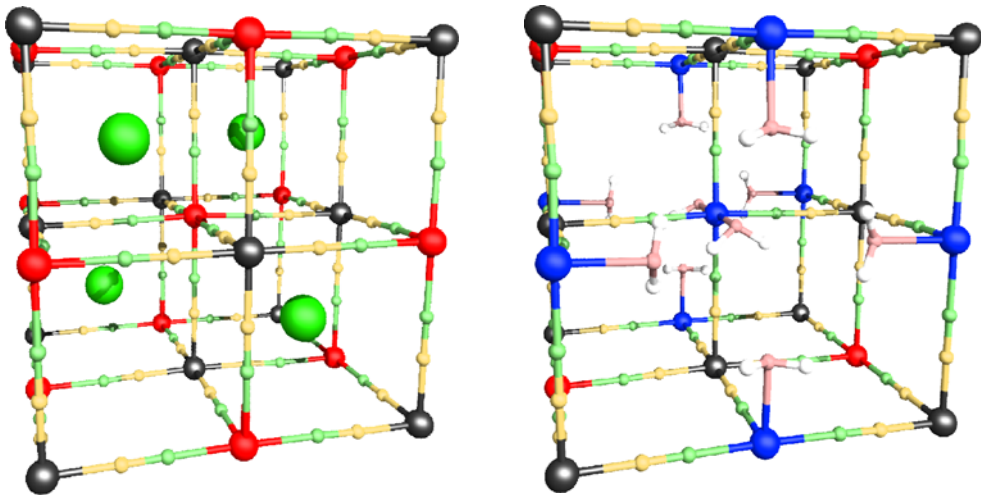

(a) $KFe[Fe(CN)_6]$ (b) $Fe_4[Fe(CN)_6]_3 \cdot 6H_2O$

Fig. 1 Unit cells of **a** "soluble" Prussian Blue (PB), and **b** "insoluble" PB used in calculations. Atoms at framework cube corners are Fe ions colour-coded depending on their crystal environment: *grey* Fe^{2+} in FeC_6 octahedra, *red* (in on-line version) Fe^{3+} in FeN_6 octahedra, *blue* Fe^{3+} in FeN_4O_2 octahedra. The same colour coding is used in density of states plots in Fig. 2 (in on-line version)

oxidation/reduction [14]. The conductivity of PB is due to two distinct phenomena: (1) thermally induced conductivity of a typical semiconductor, and (2) ionic conductivity due to the open framework form of its crystalline structure. Due to the interplay between the PB preparation route, the two conductivity modes, and the susceptibility to electrochemical oxidation and reduction, samples of PB exhibit quite complex electrochemical behaviour. In this paper, I show that purely electronic effects of PB hydration are enough to induce higher (thermally activated) conductivity of PB samples as compared to dehydrated samples. In a real experimental set-up, these will be augmented by improved ionic mobility, and the effects of interplay between electronic and ionic effects [15, 16].

PB and its analogues have been investigated theoretically using both cluster [17–19] and fully periodic models [20–23]; however, until now no fully periodic treatment of hydrated PB has been presented.

Due to the strongly correlated nature of the electronic structure of PB and its analogues, the local density approximation (LDA), and generalized gradient correction (GGA) functionals within density functional theory (DFT) have been shown to provide an incorrect description of their electronic structure [21–23]. Pure DFT approaches predict a too small band-gap, indicating either a metallic or, in the most favourable cases, a semiconducting behaviour. This failure of DFT is more general, and it is commonly attributed to the self-interaction error inherent to the local exchange functionals. It is also known to influence calculations of electronic, magnetic and structural properties of many other transition metal compounds [24, 25]. One of the proposed ad hoc corrections to the DFT has been an DFT+U method, in which the electronic Hamiltonian is augmented with a Hubbard-like term for on-site electron repulsion energy. This method was first rigorously derived for the case of LDA [26–28], and later successfully applied to correct also GGA calculations [23, 29, 30].

In this paper, the two model systems representing "soluble" and "insoluble" PB are investigated using fully periodic calculations. The influence of water on the electronic structure of the material is shown and discussed in detail. The names "soluble" and "insoluble" PB are used throughout the text to identify the models; however, the tables and figures are labelled by their respective stoichiometries to avoid confusion (note that in case of "insoluble" PB, water molecules are omitted from the formula).

Methods

The electronic structure of PB was calculated in a fully periodic manner using GGA+U methodology. We used the Dudarev et al. [28] implementation of the approach, in which the J and U terms of Hubbard Hamiltonian appear only as the difference of their respective values in a spherically symmetric way. To this end, the correction is defined in terms of $U_{eff}=U-J$ parameter, for each transition metal site. The U_{eff} values for low-spin Fe^{2+} sites and high-spin Fe^{3+} sites were set independently to 3.0 eV and 7.0 eV respectively, which was previously established to be the optimal choice for describing both the structural and electronic properties of PB [23]. All calculations were done using the PW91 exchange-correlation potential [31], and the Kohn-Sham orbitals were described using planewaves and PAW formalism [32], as implemented in VASP code [33, 34]. The total electronic energy was evaluated at a 500 eV kinetic energy cutoff, and with a 4×4×4 Monkhorst-Pack set of k-points [35]. Charge and spin densities on each

atomic site were calculated using a fast implementation of Bader analysis from fully converged charge and spin densities [36, 37]. The total magnetic moment per unit cell was found by a constrained magnetisation search through possible values, followed by an unconstrained calculation starting from the lowest energy wavefunction from previous step (a procedure that was found to be essential for finding the proper electronic ground state of PB, as detailed in [23]).

The calculation of the electronic structure of "soluble" PB ($KFe[Fe(CN)_6]$) can, in principle, be done using a primitive unit cell containing exactly a formula unit (15 atoms) [23] but, for the sake of comparison, it has been recalculated in a four times larger cubic cell (depicted in Fig. 1a). The "insoluble" PB ($Fe_4[Fe(CN)_6]_3$) was constructed by removal of one of the $Fe(CN)_6^{4-}$ complex anions together with the K^+ cations followed by introduction of six water molecules saturating the neighbouring Fe^{3+} octahedra. The unit cell of "insoluble" PB has been fully optimised with respect to ionic and lattice parameters in the cubic cell depicted in Fig. 1b. Due to the fact that the orientation of the water molecules with respect to the framework exhibits multiple local minima, an exhaustive search of possible starting orientations was conducted to find the lowest energy geometry. This was possible because, locally, each water molecule relaxes by tilting in the direction of one of the neighbouring cyanide ligands, therefore leading to four possible orientations for each water molecule. It is then found that there is a significant energetic penalty for the water molecules on the opposite walls of the cavity to be aligned in any way other than having hydrogen atoms in opposite directions. This leads to only three remaining, symmetry inequivalent orientations of water molecules, for which the total energies were calculated.

It should be noted that, in the case of both materials, the calculated structure represents only a model system of the real PB crystalline framework. The latter is often disordered, with non-periodic placement of interstitial cations and/or water-filled cavities, and with additional water molecules at interstitial sites. In the idealised models used in this study, there are three distinct Fe sites with different local geometries: (1) Fe^{2+} low-spin sites with corresponding FeC_6 octahedra, (2) Fe^{3+} high-spin sites within FeN_6 octahedra, and (3) Fe^{3+} high-spin site within FeN_4O_2 paraoctahedra. In the rest of the paper, the sites are identified by the aforementioned formulas.

Results

Crystal geometry

The calculated framework geometry of the "insoluble" form of PB is not much different from that of the "soluble" form of PB. Upon introduction of water-filled cavities, the crystalline framework undergoes a slight contraction (about 0.04 Å) and distortion from the ideal cubic cell. The defining angles of the unit cell deviate by less than 0.3° from the ideal right angles, and the *a*, *b* and *c* vectors differ from each other by about 0.01 Å. These small deviations from the ideal fcc framework are most probably due to the accuracy of the geometry optimisation convergence, and are inevitable in calculating such a large system of relatively low symmetry (note that the deviation of the cell vector lengths is of the order of 0.1%).

Similarly, the local geometry of FeC_6 and FeN_6 sites does not change significantly between "soluble" and "insoluble" PB (see Table 1). The most significant calculated difference is in the Fe–N distance as calculated for "soluble" PB and Fe–N distance at the water-substituted FeN_4O_2 site. This difference is accompanied by significant

Table 1 Calculated lattice constant (*a*) and main structural parameters of soluble and insoluble Prussian Blue (PB)

		$KFe[Fe(CN)_6]$	$Fe_4[Fe(CN)_6]_3$	Experimental
	a	10.26	10.22(±0.01)[g]	10.11[ab], 10.13[c], 10.16[d], 10.20[e]
	C–N	1.17	1.18	1.13[bf]
FeC_6	Fe–C	1.88	1.89	1.92[f] 1.94[b]
FeN_6	Fe–N	2.07	2.05	2.03[f] 2.06[b]
FeN_4O_2	Fe–N		2.04	2.02[b]
	Fe–O		2.22	1.95[b]

All distances in Å. The experimental values are giver for reference. Note that in case of experimental measurements the Fe-N distances are not distinguished between FeN_6 and FeN_4O_2 octahedra

[a] [11]
[b] [4]
[c] [39]
[d] [40]
[e] [41]
[f] [1]
[g] Average value and a maximum difference of the distorted axes

Table 2 Calculated Bader charges and spin densities of soluble and insoluble Prussian Blue

		$KFe[Fe(CN)_6]$		$Fe_4[Fe(CN)_6]_3$	
		Charge	Spin density	Charge	Spin density
FeC_6	Fe	+0.73	0.14	+0.77	0.26
	C	+1.87	0.02	+1.92	0.02
FeN_6	Fe	+1.95	4.45	+2.05	4.47
	N	−2.47	0.04	−2.47	0.04
	Fe			+1.94	4.41
FeN_4O_2	N			−2.52	0.05
	O			−1.94	0.06

electronic changes affecting the iron atom at this site, as discussed later.

The water molecules filling each cavity are located uniformly at 2.22 Å from the Fe site (Fe–O distance), which is considerably further away than the cyanide ligands. This clearly indicates a lower strength of interactions between Fe and water molecules as compared to the Fe interaction with the cyanide ligand. The optimal orientation of water molecules is such that the H_2O plane is at 102.7° to the octahedron axis, and the hydrogen atoms of the molecules at opposite sides of the cavity are pointing in opposite directions (see Fig. 1b) The oxygen atom is slightly off-centre with respect to the octahedral axis of the Fe site. All these structural effects lead to the cavity site having an inversion symmetry and, in the case of our model system with ordered cavities, also to C_{2h} symmetry of the FeN_4O_2 site. The energy differences between different arrangements of water molecules (i.e. facing each other, or pointing in opposite directions) are lower than 0.1 eV, and one has to conclude that, in finite temperature, the orientations of the molecules within the cavities will be randomly distributed.

Charge and spin distribution

Charge and spin density distribution calculated using Bader charge decomposition method is presented in Table 2. The table does not contain charges or spin densities for interstitial potassium cations and hydrogen atoms because of the negligible valence charge density at the corresponding sites. Calculated charges in both investigated forms of PB are in line with their formal Fe^{2+}, Fe^{3+} and CN^- denominations. The total magnetic moment of the ground state solution per unit cell is in both cases found to be 20 unpaired electrons, which corresponds to all four Fe^{3+} sites being in a S_z=5/2 high spin state. Small differences between "soluble" and "insoluble" PB are found mainly at these high-spin sites. The total atom projected spin density calculated for the whole high-spin octahedra (FeN_6, FeN_4O_2), calculated by adding contributions of the nearest neighbour ligand atoms, is 4.71±0.02 unpaired electrons per site in both materials. However, in case of "insoluble" PB, the spin density is slightly more delocalised to the ligands resulting in lower calculated spin density on the Fe^{3+} site itself. The atom projected spin-density in FeC_6 octahedra is low in both materials, in agreement with the diamagnetic nature of Fe^{2+} sites. The spin density at Fe^{2+} site is not strictly zero, which gives rise to the super-exchange interactions known to exist in PB analogues [18, 21].

Electronic structure

As seen in Fig. 2, despite structural similarities described above, the electronic structure of "insoluble" PB is remarkably different from its "soluble" counterpart. The band gap of "insoluble" PB is only 0.6 eV, compared to the gap of 1.7 eV of the "soluble" form. This water-cavity-induced change is accompanied by the appearance of

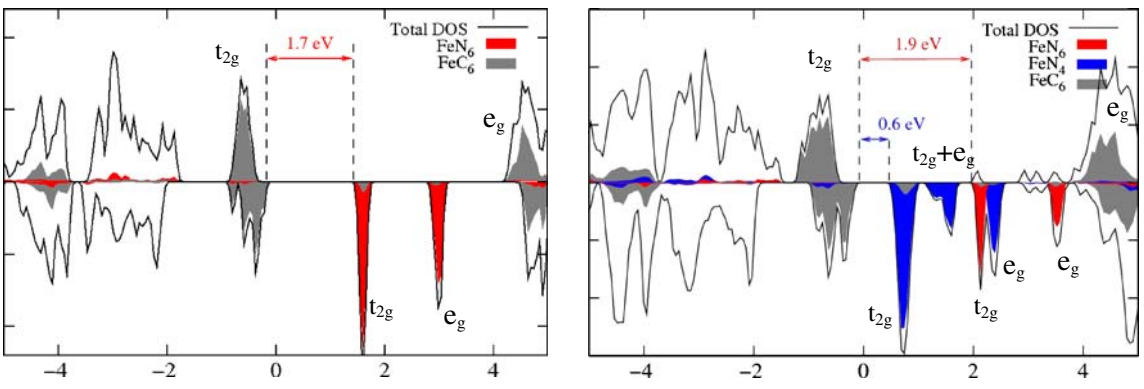

(a) $KFe[Fe(CN)_6]$ (b) $Fe_4[Fe(CN)_6]_3{\cdot}6H_2O$

Fig. 2 Calculated density of states (DOS), and atom projected DOS for **a** "soluble" and **b** "insoluble" forms of PB. Fe^{2+} to Fe^{3+} charge transfer excitation energies are given in eV for both pictures

disperse low laying unoccupied bands, instead of the very narrow bands in "soluble" PB.

The atom projected density of state (DOS) plots reveal that the FeN_6 and FeN_4O_2 have very different electronic properties within the "insoluble" PB. At the same time, the FeN_6 and FeC_6 are generally unchanged between different forms of PB. at the FeN_4O_2 sites, the *d*-electrons of the Fe^{3+} cations do not form a narrow band as in the case of fully coordinated FeN_6 sites due to the much lower ligand strength of the water molecule, as compared to the nitrogen side of CN^-. This leads to broader splitting of energies of unoccupied *d*-orbitals, and consequently to significant narrowing of the band gap of the material. Clearly separate, atom projected, *d*-bands in Fig. 2 can be identified based on their relative energies. A closed shell, fully occupied band formed by t_{2g} orbitals at the FeC_6 site is located just below the Fermi level, with the corresponding, strongly antibonding, e_g band 4 eV above in both forms of PB. The half occupied t_{2g} and e_g levels of FeN_6 and FeN_4O_2 sites are very low in energy, and are located more than 8 eV below the Fermi level. The unoccupied bands located mainly on the FeN_6 sites show a clear split between t_{2g} (lower in energy) and e_g (higher in energy) levels. The FeN_6 site of "insoluble" PB is energetically only slightly different from its equivalent in "soluble" PB. This difference manifests itself mainly in a rigid shift of band energies by 0.2 eV. In "insoluble" PB, the bottom of the unoccupied band localised on the FeN_6 site is located 1.9 eV above the Fermi level within the energy range of dispersed FeN_4O_2 bands. The equivalent band in "soluble" PB is located at 1.7 eV, and this defines the band gap of the material.

As shown in Fig. 2, the FeN_6 localised DOS also exhibits the same narrow two-band nature in both forms of PB. Therefore, a significant change in band gap between the two forms of PB is due solely to the electrons localised on FeN_4O_2 sites. At these sites, the energy levels of Fe^{3+} *d*-orbitals are spread in a series of peaks between 0.6 eV and 2.6 eV. These peaks form three separate bands, as both t_{2g} and e_g orbitals undergo splitting due to low symmetry of FeN_4O_2 paraoctahedra in "insoluble" PB. Because of this fact, the "insoluble" form of PB is predicted to have better electronic conductivity at finite temperatures than its "soluble" counterpart. At the same time, the main feature of PB—its deep blue colour, which arises from a wide absorption band around 1.75 eV—remains unchanged thanks to the accessibility of the Fe^{2+}–Fe^{3+} charge excitation between FeC_6 and FeN_6 sites independently of the exact composition of the material.

Conclusions

In the presented work, it is calculated from first principles that water-filled cavities existing in the "insoluble" form of PB induce a drastic change in the electronic structure of this material. The band gap is lowered by almost threefold, and the unoccupied bands are much more dispersed than in the case of a more symmetrical "soluble" PB. This finding is in line with known experimental data pertaining to the electronic conductivity of PB at different rates of hydration [14]. The band-gap lowering is also in line with a previously reported result obtained from ligand-field theory for a $KFe[Co(CN)_6]$ PB analogue [38]. At the same time, the structural optimisation and electron density partitioning calculations show that the structural and electronic properties of sites that are not directly neighbouring the water-filled cavity remain almost unchanged between the two forms of PB.

As Fig. 2 clearly shows, the "insoluble" PB can be seen as a superimposition of the "soluble" PB, with all its properties mostly unchanged (CT excitation energy, atomic spin moments and charges), and the hydrated part exhibiting significantly different electronic properties. Starting from this assertion, one can extrapolate to expect that properties such as absorption spectra, magnetic couplings etc. are also equivalent between the two forms of PB, with the obvious caveat that they are somewhat diluted by the lowering of the number of available FeC_6 and FeN_6 sites. The water cavities and corresponding paraoctahedral FeN_4O_2 sites can be seen as dopants affecting the properties of PB only indirectly. These results provide a first-principles theoretical confirmation of the experimentally known similarities in optical and magnetic properties within the whole range of PB stoichiometries.

Acknowledgements Financial support has been provided by Generalitat de Catalunya in form of a Beatriu de Pinós fellowship program. The author wishes to thank Ibério de P. R. Moreira, Stefan T. Bromley, and Francesc Illas from the University of Barcelona for their support and discussions, which greatly contributed to this work.

References

1. Dunbar KR, Heintz RA (1997) Prog Inorg Chem 45:283–391
2. Robin MB, Day P (1967) Adv Inorg Chem 10:247–422
3. Robin MB (1962) Inorg Chem 1:337–342
4. Herren F, Fischer P, Ludi A, Halg W (1980) Inorg Chem 19:956–959
5. Verdaguer M, Galvez N, Garde R, Desplanches C (2002) ECS Interface 11:28–33
6. Ohkoshi S-I, Hashimoto K (2002) ECS Interface 11:34–38
7. de Tacconi NR, Rajeshwar K, Lezna RO (2003) Chem Mater 15 (16):3046–3062
8. Pyrasch M, Toutianoush A, Jin W, Schnepf J, Tieke B (2003) Chem Mater 15:245–254
9. Luneau D (2001) Curr Opin Solid State Mater Sci 5:123–129
10. Ohkoshi S-I, Abe Y, Fujishima A, Hashimoto K (1999) Phys Rev Lett 82(6):1285–1288
11. Zhou P, Xue D, Luo H, Chen X (2002) Nano Lett 2:845–847
12. Moore JG, Lochner EJ, Ramsey C, Dalal NS, Stiegman AE (2003) Angew Chem Int Ed 42(24):2741–2743
13. Ksenofontov V, Levchenko G, Reiman S, Gütlich P, Bleuzen A, Escax V, Verdaguer M (2003) Phys Rev B 68:024415

14. Xidis A, Neff VD (1991) J Electrochem Soc 138:3637–3642
15. Feldman BJ, Murray RW (1986) Inorg Chem 26:1702–1708
16. Bueno PR, Giménez-Romero D, Gabrielli C, García-Jareño JJ, Perrot H, Vicente F (2006) J Am Chem Soc 128:17146–17152
17. Nishino M, Yoshioka Y, Yamaguchi K (1998) Chem Phys Lett 297:51–59
18. Harrison NM, Searle BG, Seddon EA (1997) Chem Phys Lett 266:507–511
19. Luzon J, Castro M, Vertelman EJM, Gengler RYN, van Koningsbruggen PJ, Molodtsova O, Knupfer M, Rudolf P, van Loosdrecht PHM, Broer R (2008) J Phys Chem A 112(25):5742–5748
20. Kato K, Moritomo Y, Takata M, Sakata M, Umekawa M, Hamada N, Ohkoshi S-I, Tokoro H, Hashimoto K (2003) Phys Rev Lett 91:255502
21. Middlemiss DS, Wilson CC (2008) Phys Rev B 77:155129
22. Wojdeł JC, Bromley ST (2004) Chem Phys Lett 397:154–159
23. Wojdeł JC, Moreira I de PR, Bromley ST, Illas F (2008) J Chem Phys 128:044713
24. de PR Moreira I, Illas F, Martin RL (2002) Phys Rev B 65:155102–14
25. Moreira I de PR, Dovesi R (2004) Int J Quantum Chem 99:805
26. Liechtenstein AI, Anisimov VI, Zaanen J (1995) Phys Rev B 52: R5467
27. Anisimov VI, Aryasetiawan F, Lichtenstein AI (1997) J Phys Condens Matter 9:767
28. Dudarev SL, Botton GA, Savrasov SY, Humphreys CJ, Sutton AP (1998) Phys Rev B 57:1505
29. Madsen GKH, Novsk P (2005) Europhys Lett 69:777
30. Loschen C, Carrasco J, Neyman KM, Illas F (2007) Phys Rev B 75:035115
31. Perdew JP, Chevary JA, Vosko SH, Jackson KA, Pederson MR, Singh DJ, Fiolhais C (1992) Phys Rev B 46:6671–6687
32. Blöchl PE (1994) Phys Rev B 50:17953–17979
33. Kresse G, Furthmüller J (1996) Phys Rev B 54:11169–11186
34. Kresse G, Joubert D (1999) Phys Rev B 59:1758–1775
35. Monkhorst HJ, Pack JD (1976) Phys Rev B 13:5188–5192
36. Bader RFW (1990) Atoms in molecules: a quantum theory. Oxford University Press, New York
37. Henkelman G, Arnaldsson A, Jónsson H (2006) Comput Mater Sci 36:254–360
38. Kawamoto T, Asai Y, Abe S (1999) Phys Rev B 60:12990–12993
39. Nakanishi S, Lu G, Kothari HM, Bohannan EW, Switzer JA (2003) J Am Chem Soc 125(49):14998–14999
40. Schwudke D, Stosser F, Scholz R (2000) Electrochem Commun 2:301–306
41. Tennakone K, Dharmaratne WGD (1983) J Phys C 16:5633–5639